COMMUNICATION

CrossMark
click for updates

A long-term corrosion barrier with an insulating boron nitride monolayer†

Liting Shen,‡[a] Yuda Zhao,‡[ab] Yi Wang,[a] Ruobing Song,[a] Qian Yao,[c] Shanshan Chen*[d] and Yang Chai*[ab]

Graphene has been demonstrated as an ultrathin and light-weight corrosion barrier because of its high impermeability. However, it fails to prevent the Cu corrosion over a long term because the high conductivity of graphene enables the formation of a galvanic cell and promotes the electrochemical reaction. Here we theoretically and experimentally study a boron nitride (BN) monolayer as a long-term corrosion barrier for Cu. Our density functional theory calculations show that the potential barrier for O_2 to pass through BN is close to that of graphene. The long-term barrier characteristics of BN and graphene are comparably evaluated by aging in an ambient environment for 160 days. Morphological and spectroscopic characterization shows that a BN monolayer has much better long-term barrier performance than graphene. X-ray photoelectron spectroscopy analysis shows that the Cu^{2+} percentage of the aging Cu sample with a BN barrier is reduced by around 15 times compared with that covered by graphene. The superior long-term barrier performance of a BN monolayer can be understood to be a result of its high impermeability and insulating characteristics, which suppress the galvanic corrosion under the ambient environment. These studies reveal that a BN monolayer is a more effective long-term corrosion barrier than graphene.

[a]Department of Applied Physics, The Hong Kong Polytechnic University, Hung Hom, Kowloon, Hong Kong, People's Republic of China. E-mail: ychai@polyu.edu.hk

[b]The Hong Kong Polytechnic University Shenzhen Research Institute, Shenzhen, People's Republic of China

[c]Department of Physics, Xiamen University, Xiamen, People's Republic of China

[d]Department of Physics, Renmin University of China, Beijing, People's Republic of China. E-mail: sschen@xmu.edu.cn

1. Introduction

Metal corrosion in infrastructures caused an annual loss of around \$300 billion in the United States and €200 billion in Europe in 2014.[1] It is highly desirable to develop an ultrathin corrosion barrier, which can effectively protect a metal for a long term but insignificantly affect the intrinsic properties of the materials that are protected. Graphene, an atomic-level thin layer, has been demonstrated as a corrosion barrier for metals including Ni,[2] Cu,[2–5] Ag,[6–8] Au[9] and Pt[10,11] and as a diffusion barrier for a metal–semiconductor interconnect.[12–15] High-temperature annealing and electrochemical test showed excellent barrier performance of a graphene nanosheet for a short term.[2,16–18] However, Zhou et al. and Schriver et al. revealed that a graphene barrier promotes the corrosion of Cu in air when the exposure time is extended to several months.[19,20] This corrosion-promotion process by the graphene barrier has been understood to be the result of the galvanic corrosion of the graphene–Cu couple.[19,20] An electrochemical path is established in the graphene/oxide/Cu stack and gives rise to a corrosion rate even higher than that of bare Cu. Therefore, the inhibition of the corrosion lies in the suppression of the electrochemical reaction paths. Researchers have incorporated multilayer graphene oxides or graphene into insulating polymer matrixes to inhibit the electrochemical reaction and enhance the barrier performance.[3,21–25] However, it involves a complex process and increases the barrier thickness.

Hexagonal boron nitride (BN) has a lattice structure similar to graphene,[26] ultrathin thickness, high resistivity,[27] excellent thermal conductivity,[28] air-stability,[29,30] and high impermeability.[9,31–33] Liu et al. showed excellent barrier performance of BN, which can effectively protect Ni from oxidation at the temperature of 1100 °C for a short term.[32] Li et al. demonstrated strong oxidation resistance of BN sheets on short-term heating.[30] Researchers also studied the corrosion-resistance of BN coated Cu foil for 200 hours, and revealed that the BN coating increases the open circuit potential of Cu foil.[34] However, the long-term anti-corrosion performance of the BN barrier has

remained unexplored at the current stage. Also, the barrier performance of BN and graphene has not been comparatively studied yet.

In this work, we perform first-principles calculations to theoretically evaluate the impermeability of a BN monolayer to oxygen. The barrier performance of BN and graphene is experimentally compared by electrochemical, morphological, and spectroscopic characterization. Monolayer BN shows much better long-term corrosion barrier performance than graphene, which is attributed to the inhibition of galvanic reaction because of high insulating properties of BN.

2. Experiment details

The self-consistent field calculation was conducted with a Quantum ESPRESSO.[35] The distances between a graphene/BN plane and an oxygen molecule varied from 2.78 Å to 0 Å. The 4×4 conventional unit cell was used for graphene and BN. The convergence threshold on total energy is 10^{-6} and the one on forces is 10^{-3} (both in a.u.). The kinetic energy cutoff for wavefunctions was 50 Ry (Rydberg unit of energy, 1 Ry = 13.6 eV), and the kinetic energy cutoff for charge density and potential was 200 Ry.

The electrochemical characterization was performed by a CHI660 electrochemical workstation. A BN/Cu, G/Cu or b/Cu sample was used as the working electrode with a graphite bar as the counter electrode and a calomel electrode as the reference electrode. The electrolyte was 0.1 M NaCl solution. For Tafel analysis, the scanning rate was 10 mV s^{-1} and the scan step was 1 mV. A small voltage perturbation (10 mV) was used in the EIS measurement. The EIS results were analysed with Zview software.

Bare Cu foil (bCu), G/Cu and BN/Cu were dipped into a 1.0 M HNO$_3$ solution for 15 min. The SEM characterization and the energy dispersive X-ray spectroscopy (EDS) were conducted using a JEOL Model JSM-6490 microscope. The acceleration voltage was kept at 20 kV and the working distance was 10 mm.

The BN/Cu and G/Cu were exposed to the ambient environment for 160 days. The surface morphologies of the samples were studied with optical microscope (OM, Leica DM1750M) and SEM. The corroded Cu samples were characterized by Raman, SEM and XPS methods. A Raman spectrometer with an excitation wavelength of 488 nm was used to study the atomic vibration of Cu oxides. The power of the laser was 50 mW. A Lorentzian peak fitting method was applied to find the peak height for the peak at 218 cm^{-1}. For XPS, all scans were performed with the angle between the normal of the thin Cu foil and the detector fixed at 45°. The step of the scanning was 0.25 eV. The deconvolution was done using XPSPEAK4.1 software. A Shirley background was used for the curve fitting. The X-ray diffraction (XRD) data were acquired using a Rigaku SmartLab diffractometer with the scanning step of 0.1 degree. For the samples after 160 day aging, the peaks around 61.7 (PDF# 65-3288), 65.9 (PDF# 48-1548), and 66.5 (PDF# 48-1548) degrees can be classified to Cu$_2$O (220), CuO (022) and CuO (310) structures, respectively.

3. Results and discussions

3.1 Density functional theory calculations

Theoretical calculations have been extensively performed to show the impermeability of graphene to most of the molecules, atoms, and ions.[36–39] However, the barrier potential for O$_2$ to pass through BN layers has not been calculated. The potential barrier for O$_2$ to pass through graphene and BN was calculated through the density functional theory (DFT). Fig. 1a shows that the potential barriers for O$_2$ through the "hollow" site of BN and graphene are around 30 eV and 35 eV, respectively. This extremely high potential barrier prohibits O$_2$ from passing through the "hollow" site of BN or graphene. The calculation results for the "bridge" site (Fig. 1b) show that the potential barrier is quite large, around 100 eV for both BN and graphene. Our first-principles calculations show high impermeability of BN barriers comparable to that of graphene.

When O$_2$ approaches the graphene or BN surface, the dense electron cloud of the two-dimensional (2D) barrier layer forms a strong repelling field and blocks the O$_2$ translocation. In Fig. 1a and b, we find that the potential barriers of graphene are higher than those of BN by ~5 eV on both "hollow" and "bridge" sites. We attribute this to the electron density difference between graphene and BN. Owing to the different element configurations and crystal parameters in graphene and BN, the electrons of graphene are relatively uniformly distributed, while the electron clouds in BN are densely distributed around N atoms.[40] At the "bridge" site, the electron density of graphene is higher than that of BN, and the "hollow" site of BN has larger "pore" and lower electron density than graphene. In addition, the potential barrier at the "bridge" site is almost three times larger than that at the "hollow" site, because of the presence of much higher electron density at the "bridge" site. The potential barriers of graphene and BN for O$_2$ are both 2 and 3 magnitudes greater than the thermal energy of O$_2$ (26 meV) at room
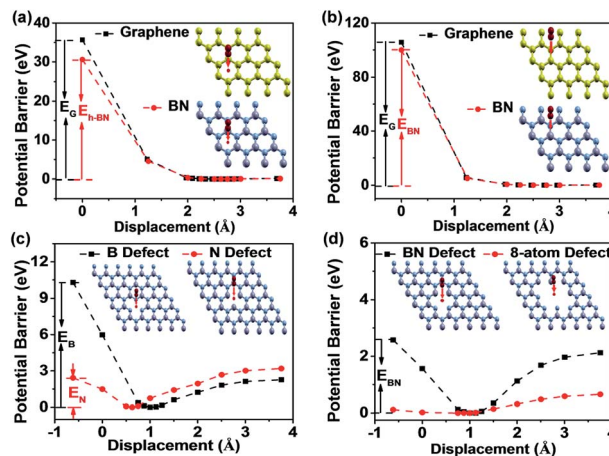

Fig. 1 Potential barriers of O$_2$ penetrating through (a) the "hollow" sites and (b) the "bridge" sites of graphene and BN. (c) The potential barrier of O$_2$ passing through BN with single B-atom or N-atom defect. (d) The potential barrier of O$_2$ through a BN plane with one B–N defect and 8-atom defects.

This journal is © The Royal Society of Chemistry 2016

J. Mater. Chem. A, 2016, 4, 5044–5050 | 5045

temperature. Thus, it is reasonable to expect that the graphene and BN are both good O_2 barrier materials.

The B/N stoichiometry of the BN by the CVD method is generally less than 1 in XPS analysis.[41,42] For the CVD grown BN on copper foil, the defective sites in BN allow O_2 to react with Cu and result in oxidation.[34] Here we use DFT calculations to study the impermeability of defected BN against O_2. For single-atom defect of BN, there are two possible defective sites, namely single B-atom defect and N-atom defect. The inset of Fig. 1c shows the schematic diagram of the defective BN barrier, where an O_2 molecule vertically passes through the defective BN plane. The potential barriers for the BN with single B-atom and single N-atom are different. For the BN with a single B-atom defect, the potential barrier increases as O_2 approaches the BN plane, as depicted in Fig. 1c. The barrier height is around 11 eV, much greater than the thermal energy of O_2 at room temperature. The BN monolayer with single B-atom defect is still impermeable to O_2. For the BN with single N-atom defect, the barrier height is about 3 eV (Fig. 1c). This indicates that O_2 also has a low probability of passing through the BN plane. The different results of the two types of defects can be explained by the electron structures of B and N. A N atom has greater electron density than a B atom.[40] In the case of single B-atom defect, the dense electron cloud of the three surrounding N atoms overlaps with the electrons of O_2 and induces the large barrier potential. For the single N-atom defect case, the energy is lowered because the N atom with higher electron density is removed. We also performed DFT calculation for the BN monolayer with one pair of B–N defect (Fig. 1d). The minimum potential point is around 1 Å away from the basal plane and the potential barrier is around 2 eV. Compared with the results for single B-atom defect, the sample with one pair of B–N defect has lower barrier energy. We further expand the defect sites, as shown in Fig. 1d. For the 8-atom defect situation, the barrier height is lowered to around 0.1 eV, which means that the highly defective BN surface is not an effective barrier against O_2.

3.2 Short-term corrosion test

Monolayer graphene and BN were fabricated by the chemical vapour deposition (CVD) method on Cu foil. The characterization of monolayer graphene and BN by Raman spectroscopy (HORIBA HR800), X-ray photoelectron spectroscopy (XPS, ULVAC-PHI Quantum 2000) and atomic force microscopy (AFM, SPA-400) can be found in Fig. S1 and S2.† The Raman peak of BN is located around 1369 cm^{-1}, in agreement with the previous results on monolayer BN.[43,44] The XPS spectrum shows that the N/B ratio is around 1.07. The thickness of the BN is measured by AFM, less than 0.52 nm. These results demonstrate high-quality monolayer graphene and BN.

We first conducted an acidic corrosion test to evaluate the barrier performance of graphene and BN monolayer. Bare Cu foil (bCu) and Cu foils with graphene (G/Cu) and with BN (BN/Cu) coating were dipped into a HNO_3 solution. The scanning electron microscopy (SEM) images, and XPS and Raman spectra of the samples before and after the corrosion test are shown in

Fig. S3.† The results exhibit that graphene and BN can effectively protect the underlying Cu foil for a short-term.

An electrochemical corrosion test was conducted to quantitatively compare the barrier performance of the graphene and BN samples in a relatively short term. The corrosion penetration rates (CPR) of G/Cu, BN/Cu and bCu samples are calculated according to the equation:[45]

$$CPR(\text{mm per year}) = 0.327 \times \frac{10^{-3} M i_{corr}}{m\rho} \quad (1)$$

where M is the molar mass (g mol^{-1}), m is the valence, ρ is the density of the material (g cm^{-3}), and i_{corr} is the corrosion current density (mA m^{-2}). The corrosion current densities are about 40.0, 31.3 and 316 mA m^{-2}, and the extracted CPR values are about 0.036, 0.046 and 0.360 mm per year for the G/Cu, BN/Cu and bCu samples, respectively. The corrosion resistance of the G/Cu and BN/Cu are similar. The small E_{corr} shift (Fig. 2a) also indicates that the susceptibilities of the G/Cu and BN/Cu samples to the electrochemical oxidation are approximately the same.[18] Graphene shows a significant passivation effect in short-term heating test[2] and electrochemical test.[16–18] The mass transport through the BN or graphene lattice becomes a rate limiting factor of corrosion due to their high impermeability.

We found that the equilibrium potential (E_{eq}) shifts to the positive direction by around 50 mV when the graphene or BN barriers are present, as shown in Fig. S4.† This feature has also been reported by Prasai et al. and Raman et al.[17,18] The positive shift can be caused by the Cu concentration difference at the working electrodes. Under low concentration conditions, the Nernst half-cell equations can be expressed as:[46]

$$E_{eq} = E_{eq}^0 + \frac{59}{m} \log(n_{ions}) \quad (2)$$

where E_{eq} is the equilibrium potential, E_{eq}^0 is the equilibrium potential under standard conditions, m is the valence number (2 for Cu^{2+} and 1 for Cu$^+$), and n_{ions} is the concentration of Cu ions between 2D barrier layer and Cu. It is found that the concentration of the Cu ions in the G/Cu and BN/Cu samples is 50 times as much as that in the bCu sample. The Cu ions are generated by the galvanic corrosion. However, the 2D barrier inhibits the migration of Cu ions through it, and prevents the
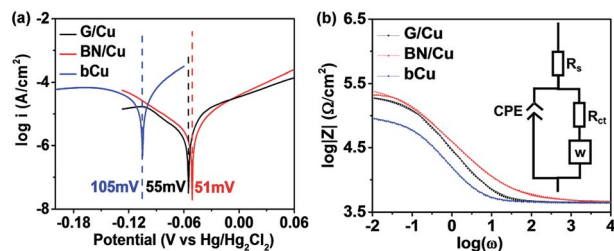

Fig. 2 (a) The Tafel plot of the BN/Cu, G/Cu, and bCu samples. The equilibrium potential shifts to the positive direction by around 50 mV when the graphene or BN barrier is present. (b) The electrochemical impedance spectroscopy (EIS) curve measured for the bCu, BN/Cu and G/Cu samples. The inset schematic diagram shows the corresponding Randles–Warburg model.

5046 | *J. Mater. Chem. A*, 2016, **4**, 5044–5050

This journal is © The Royal Society of Chemistry 2016

formation of oxides. Thus, the Cu ions accumulate between the 2D barrier and Cu, and the concentration of Cu ions at the interface increases accordingly, which further retards the electrochemical reaction.

The Randles–Warburg model can be used to explain the corrosion mechanism of uncoated metals. We use the model for the BN/Cu and G/Cu samples, as shown in the equivalent circuit in Fig. 2b,[17] where R_s is the solution resistance, and CPE (constant phase element) represents the capacitance between the metal and the solution. We can translate the CPE to double layer capacitance (C_{dl}). A Warburg element (W) accounts for the semi-infinite diffusion between thin Cu foil and electrolyte. R_{ct} is the resistance due to the charge transfer between the metal and the solution.[17,47]

According to Wang *et al.*, the protective coatings with high R_{ct} and low C_{dl} values are considered to provide good anticorrosion performance, because R_{ct} measures the resistance to aggressive species transfer, and C_{dl} reflects the water uptake tendency of coatings.[47,48] The extracted C_{dl} and R_{ct} parameters according to the model are documented in Table S1.† The C_{dl} of the BN/Cu (3.3×10^{-6} F cm^{-2}) and G/Cu (1.7×10^{-5} F cm^{-2}) samples is lower than that of the bCu samples (5.3×10^{-5} F cm^{-2}) by around 16 times and 3 times, respectively. One possible explanation for the significant C_{dl} difference is that the G/Cu or BN/Cu structure forms another capacitor in series with the capacitor formed by the electrolyte–electrode interface.[17] The R_{ct} of the G/Cu (1.75×10^5 Ω cm^{-2}) and BN/Cu (2.79×10^5 Ω cm^{-2}) samples is greater than that of the bCu samples (7.71×10^4 Ω cm^{-2}) by around 2 times and 4 times, respectively, showing the high resistivity of BN and graphene layers to corrosion.

3.3 Long-term corrosion test

The foregoing studies have shown that BN exhibits a corrosion barrier performance similar to that of graphene in a short term. To evaluate the long-term corrosion barrier characteristics, the as-grown G/Cu and BN/Cu samples were kept in the ambient environment at room temperature with a relative humidity of around 60% for 160 days. Fig. 3a and b are representative optical microscopy (OM) images of the as-prepared G/Cu and BN/Cu samples, showing uniformly coloured and highly reflective surfaces. This indicates that these two kinds of as-prepared samples are free of oxides in the initial stage of the corrosion test. The morphologies of the as-prepared G/Cu and BN/Cu samples are quite similar to that of the bCu sample because of high optical transmittance of both graphene and BN. However, after a certain period of the corrosion test, the G/Cu and BN/Cu samples exhibit distinguished appearances. Fig. 3c shows a representative OM image of the G/Cu sample after exposure to the ambient environment for 80 days, which exhibits highly inhomogeneous corrosion, agreeing well with previous reports.[19,20] The Cu corrosion is initiated from the defective sites of the graphene barrier. Around 65% of the observed area is corroded. In contrast, the BN/Cu sample remains protected with few Cu grains showing different colours (Fig. 3d). For the G/Cu sample after 120 day corrosion (Fig. 3e),
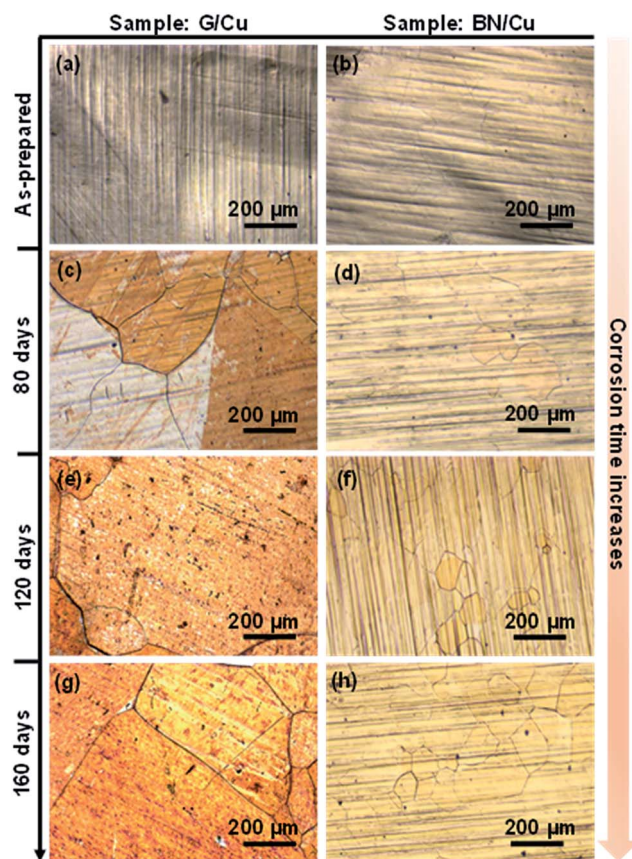

Fig. 3 Optical microscopy images of G/Cu and BN/Cu. (a and b) As-prepared samples, (c and d) after 80 days', (e and f) after 120 days' and (g and h) after 160 days' exposure to the ambient environment.

most of the areas are severely corroded, showing a different morphology from Fig. 3a. A few grains of the BN/Cu sample show colour changes but the surface structure of the BN/Cu can still be viewed, as depicted in Fig. 3f. The corroded area occupies about 6% of the whole sample. Compared with the G/Cu sample (Fig. 3g), the BN/Cu sample shows much less colour change after aging for 160 days, as evidenced in Fig. 3h, almost indistinguishable from the as-prepared BN/Cu sample. The lightly corroded area consists of 10% of the observed region. These results imply that the BN/Cu is less severely oxidized than the G/Cu after the long-term corrosion test, and BN is an effective long-term corrosion barrier for Cu.

Fig. 4a and b show typical SEM images of the as-prepared G/Cu and BN/Cu samples. The relatively smooth surface can be viewed, in agreement with our optical image characterization. Fig. 4c shows the SEM image of the G/Cu surface after 80 day aging. The grain boundary in the middle separates the figure into two parts. In the left region, some small white regions can be observed, which is different from the morphology of Fig. 4a due to the oxidation. In Fig. 4d, we find that most of the area is homogeneously colored with a small region at the lower left hand side non-uniformly colored. After exposure to the ambient environment for 120 days and 160 days, the black-white regions consist of most of the G/Cu sample and can be clearly viewed (Fig. 4e and g). Based on the morphology change, almost all the
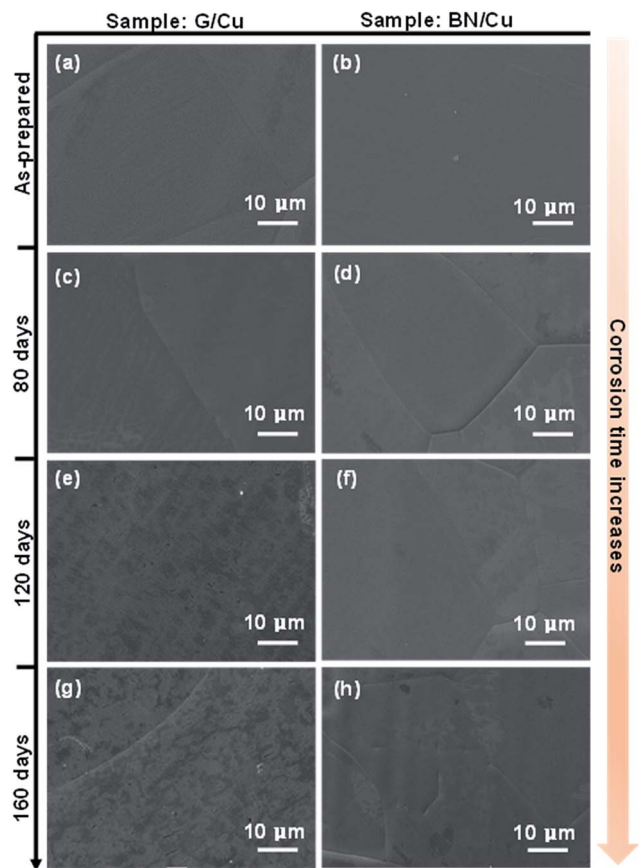
This journal is © The Royal Society of Chemistry 2016

J. Mater. Chem. A, 2016, **4**, 5044–5050 | **5047**

Fig. 4 Scanning electron microscopy images of the G/Cu and the BN/Cu samples. (a and b) As-prepared samples, (c and d) after 80 days', (e and f) after 120 days' and (g and h) after 160 days' exposure to the ambient environment.
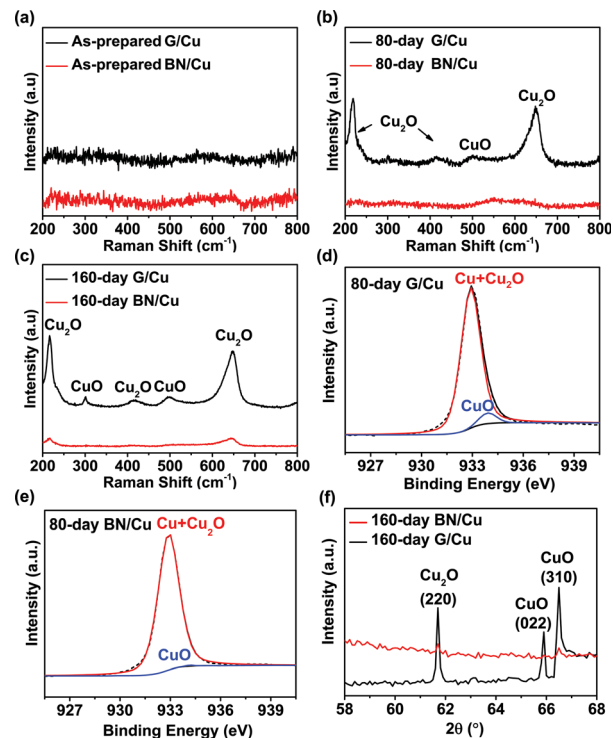

Fig. 5 Raman spectra of G/Cu and BN/Cu samples: (a) as-prepared, (b) 80 day aging, and (c) 160 day aging. XPS spectra of (d) the G/Cu sample and (e) the BN/Cu sample after 80 day aging with peak deconvolution. (f) XRD graph of the G/Cu and BN/Cu samples after 160 day aging.

detected area is found to be severely oxidized. The surface inhomogeneity is very likely to be caused by the formation of Cu oxides according to this series of observation. This indicates that G/Cu is more severely oxidized than BN/Cu. For the BN/Cu after long-term exposure, the surface is still relatively homogeneous with little black-white mixed regions (Fig. 4f and h). These striking differences show that BN/Cu is more resistant to corrosion in an ambient environment than G/Cu.

The Raman spectra of the G/Cu and BN/Cu were monitored during the long-term corrosion tests, as shown in Fig. 5a–c. From the Raman spectrum of the as-prepared sample in Fig. 5a, we can observe negligible peaks of Cu oxides, indicating that the as-prepared G/Cu and BN/Cu samples are almost pristine, exhibiting good consistency with our optical and SEM characterization. Fig. 5b shows the Raman spectrum after 80 day exposure to ambient conditions. Two pronounced peaks at 218 cm^{-1} and 644 cm^{-1} can be detected on the G/Cu sample, corresponding to the Cu_2O peaks.[49] In contrast, insignificant changes can be observed for the BN/Cu sample at this stage. After 160 day exposure to the ambient environment, more Raman peaks emerge for the G/Cu sample, as shown in Fig. 5c. The peaks at 218 cm^{-1}, 414 cm^{-1} and 644 cm^{-1} correspond to the Cu_2O peaks,[49] and the peaks at 300 cm^{-1} and 500 cm^{-1}

result from CuO.[50] Although the Cu_2O peaks at 218 cm^{-1} and 644 cm^{-1} are also observed in the BN/Cu sample after 160 day exposure, the intensity is much weaker than that in the G/Cu sample.

Fig. 5d and e show representative XPS data of the G/Cu and BN/Cu samples after 80 day exposure. The binding energy of Cu^{2+} is 933.9 eV, around 1 eV greater than that of Cu atoms and Cu^+.[51] The Cu^{2+} percentage of the G/Cu sample is 3% (Fig. 5d), comparable to the result reported by Zhou et al.[20] In comparison, the Cu^{2+} percentage drops to 0.2% for the BN/Cu sample (Fig. 5e). Similar XPS results were also obtained for 160 day samples, as shown in Fig. S5.† The X-ray diffraction (XRD) has a higher penetration depth than the XPS method. Fig. 5f shows the XRD patterns of the G/Cu and BN/Cu samples after 160 day aging. In the G/Cu sample, the peaks around 61.7, 65.9, and 66.5 degrees can be assigned to Cu_2O (220), CuO (022) and CuO (310), respectively. However, for the BN/Cu sample, insignificant peaks of oxide can be observed. These results confirm that the BN/Cu sample is better protected after long-term corrosion.

3.4 Anti-corrosion mechanisms of a BN barrier

The oxidation of Cu thin films at room temperature was previously studied by Cabrera et al.[52] Cu functions as a cathode in the electrochemical cell, providing electrons to ionize oxygen molecules and forming oxides at the surface of Cu. The electrons tunnel through the oxide layer on the Cu surface and react
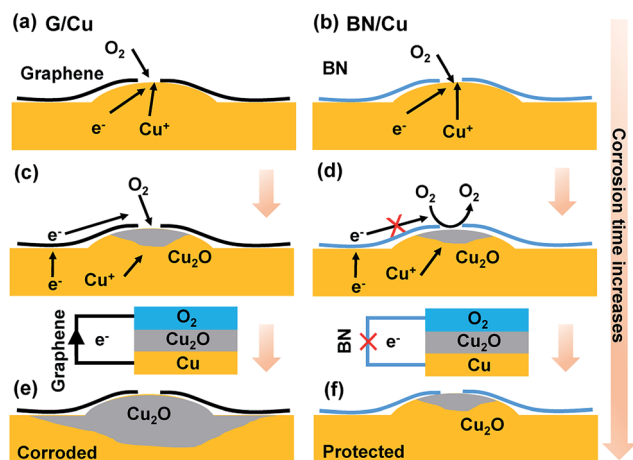
5048 | *J. Mater. Chem. A*, 2016, **4**, 5044–5050

This journal is © The Royal Society of Chemistry 2016

Fig. 6 Schematic diagrams of the corrosion mechanisms in the BN/Cu and G/Cu samples. The defective sites in the (a) graphene and (b) BN samples allow the unprotected Cu to react with O_2 and eventually form oxides for both the G/Cu and BN/Cu samples. (c) The highly conductive graphene can transport electrons to oxygen atoms, working as the cathode in the electrochemical circuit. (d) The electrochemical circuit for the BN/Cu sample is open because BN is electrically insulating. Equivalent circuit for the (e) G/Cu and (f) BN/Cu samples.

with oxygen. The electron tunnelling is highly dependent on the oxide depth. The oxidation rate slows down significantly as the thickness of the insulating oxidation layer increases, because few electrons can tunnel through the oxidation layer to complete the reaction.

For the G/Cu and BN/Cu samples, the defective sites in the 2D barrier allow the unprotected Cu to react with O_2 and form oxides (Fig. 6a and b). For both samples, the transport of electrons through Cu is blocked as the Cu_2O layer grows. However, the graphene barrier provides another conduction path for electrons to reach oxygen because it possesses high electrical conductivity. The conductivity of graphene is significantly higher than that of BN in the horizontal direction. The highly conductive graphene can transport electrons to oxygen atoms, working as the cathode for the galvanic reaction (Fig. 6c). The corrosion region expands in both horizontal and vertical directions, as illustrated in Fig. 6e. For the BN/Cu sample, the electron transport in the horizontal direction is prohibited because it is electrically insulating, in which the close loop of an electrochemical cell is disconnected and the corrosion is slowed down, as depicted in Fig. 6d and f. Therefore, the BN/Cu shows higher oxidation resistance than the G/Cu.

4.   Conclusions

Our theoretical calculation predicts that BN has impermeability similar to that of graphene. An electrochemical test verifies that both BN and graphene have excellent short-term corrosion resistance. We comparably evaluate the long-term corrosion resistance of BN and graphene for 160 days. The OM, SEM, Raman, XPS and XRD characterization results show that a BN monolayer has much better long-term corrosion resistance than that of graphene. This excellent barrier performance of a BN

monolayer can be understood to be a result of its high insulating characteristics, suppressing the electrochemical reaction. The BN layers can be considered as an alternative ultra-thin barrier to graphene when the conductivity of the protection layer is not important for the application of the device.

Acknowledgements

Notes and references

1 S. Bohm, *Nat. Nanotechnol.*, 2014, **9**, 741–742.
2 S. Chen, L. Brown, M. Levendorf, W. Cai, S.-Y. Ju, J. Edgeworth, X. Li, C. W. Magnuson, A. Velamakanni, R. D. Piner, J. Kang, J. Park and R. S. Ruoff, *ACS Nano*, 2011, **5**, 1321–1327.
3 D. Kang, J. Y. Kwon, H. Cho, J. H. Sim, H. S. Hwang, C. S. Kim, Y. J. Kim, R. S. Ruoff and H. S. Shin, *ACS Nano*, 2012, **6**, 7763–7769.
4 Y. P. Hsieh, M. Hofmann, K. W. Chang, J. G. Jhu, Y. Y. Li, K. Y. Chen, C. C. Yang, W. S. Chang and L. C. Chen, *ACS Nano*, 2014, **8**, 443–448.
5 Y. D. Zhao, Y. Z. Xie, Z. K. Liu, X. S. Wang, Y. Chai and F. Yan, *Small*, 2014, **10**, 4521–4542.
6 Y. Zhao, Y. Xie, Y. Y. Hui, L. Tang, W. Jie, Y. Jiang, L. Xu, S. P. Lau and Y. Chai, *J. Mater. Chem. C*, 2013, **1**, 4956–4961.
7 Y. Zhao, Y. Xie, Z. Bao, Y. H. Tsang, L. Xie and Y. Chai, *J. Phys. Chem. C*, 2014, **118**, 11827–11832.
8 J. C. Reed, H. Zhu, A. Y. Zhu, C. Li and E. Cubukcu, *Nano Lett.*, 2012, **12**, 4090–4094.
9 Q. Cai, L. H. Li, Y. Yu, Y. Liu, S. Huang, Y. Chen, K. Watanabe and T. Taniguchi, *Phys. Chem. Chem. Phys.*, 2015, **17**, 7761–7766.
10 L. Nilsson, M. Andersen, R. Balog, E. Laegsgaard, P. Hofmann, F. Besenbacher, B. Hammer, I. Stensgaard and L. Hornekaer, *ACS Nano*, 2012, **6**, 10258–10266.
11 H. Kim, A. W. Robertson, S. O. Kim, J. M. Kim and J. H. Warner, *ACS Nano*, 2015, **9**, 5947–5957.
12 C. G. Kang, S. K. Lim, S. Lee, S. K. Lee, C. Cho, Y. G. Lee, H. J. Hwang, Y. Kim, H. J. Choi, S. H. Choe, M.-H. Ham and B. H. Lee, *Nanotechnology*, 2013, **24**, 115707.
13 Y. Zhao, Z. Liu, T. Sun, L. Zhang, W. Jie, X. Wang, Y. Xie, Y. H. Tsang, H. Long and Y. Chai, *ACS Nano*, 2014, **8**, 12601–12611.
14 C. P. Y. Wong, T. J. H. Koek, Y. P. Liu, K. P. Loh, K. E. J. Goh, C. Troadec and C. A. Nijhuis, *ACS Appl. Mater. Interfaces*, 2014, **6**, 20464–20472.
15 W. K. Morrow, S. J. Pearton and F. Ren, *Small*, 2015, **12**, 120–134.

16 N. T. Kirkland, T. Schiller, N. Medhekar and N. Birbilis, *Corros. Sci.*, 2012, **56**, 1–4.

17 D. Prasai, J. C. Tuberquia, R. R. Harl, G. K. Jennings and K. I. Bolotin, *ACS Nano*, 2012, **6**, 1102–1108.

18 R. K. S. Raman, P. C. Banerjee, D. E. Lobo, H. Gullapalli, M. Sumandasa, A. Kumar, L. Choudhary, R. Tkacz, P. M. Ajayan and M. Majumder, *Carbon*, 2012, **50**, 4040–4045.

19 M. Schriver, W. Regan, W. J. Gannett, A. M. Zaniewski, M. F. Crommie and A. Zettl, *ACS Nano*, 2013, **7**, 5763–5768.

20 F. Zhou, Z. Li, G. J. Shenoy, L. Li and H. Liu, *ACS Nano*, 2013, **7**, 6939–6947.

21 Y.-H. Yang, L. Bolling, M. A. Priolo and J. C. Grunlan, *Adv. Mater.*, 2013, **25**, 503–508.

22 O. C. Compton, S. Kim, C. Pierre, J. M. Torkelson and S. T. Nguyen, *Adv. Mater.*, 2010, **22**, 4759–4763.

23 W. Sun, L. Wang, T. Wu, M. Wang, Z. Yang, Y. Pan and G. Liu, *Chem. Mater.*, 2015, **27**, 2367–2373.

24 H. Kim, Y. Miura and C. W. Macosko, *Chem. Mater.*, 2010, **22**, 3441–3450.

25 K. Choi, S. Nam, Y. Lee, M. Lee, J. Jang, S. J. Kim, Y. J. Jeong, H. Kim, S. Bae, J. B. Yoo, S. M. Cho, J. B. Choi, H. K. Chung, J. H. Ahn, C. E. Park and B. H. Hong, *ACS Nano*, 2015, **9**, 5818–5824.

26 C. R. Dean, A. F. Young, I. Meric, C. Lee, L. Wang, S. Sorgenfrei, K. Watanabe, T. Taniguchi, P. Kim, K. L. Shepard and J. Hone, *Nat. Nanotechnol.*, 2010, **5**, 722–726.

27 K. Watanabe, T. Taniguchi and H. Kanda, *Nat. Mater.*, 2004, **3**, 404–409.

28 D. Golberg, Y. Bando, Y. Huang, T. Terao, M. Mitome, C. Tang and C. Zhi, *ACS Nano*, 2010, **4**, 2979–2993.

29 Y. Chen, J. Zou, S. J. Campbell and G. Le Caer, *Appl. Phys. Lett.*, 2004, **84**, 2430–2432.

30 L. H. Li, J. Cervenka, K. Watanabe, T. Taniguchi and Y. Chen, *ACS Nano*, 2014, **8**, 1457–1462.

31 E. Husain, T. N. Narayanan, J. J. Taha-Tijerina, S. Vinod, R. Vajtai and P. M. Ajayan, *ACS Appl. Mater. Interfaces*, 2013, **5**, 4129–4135.

32 Z. Liu, Y. Gong, W. Zhou, L. Ma, J. Yu, J. C. Idrobo, J. Jung, A. H. MacDonald, R. Vajtai, J. Lou and P. M. Ajayan, *Nat. Commun.*, 2013, **4**, 2541.

33 M. Yi, Z. Shen, X. Zhao, S. Liang and L. Liu, *Appl. Phys. Lett.*, 2014, **104**, 143101.

34 L. H. Li, T. Xing, Y. Chen and R. Jones, *Adv. Mater. Interfaces*, 2014, **1**, 1300132.

35 P. Giannozzi, S. Baroni, N. Bonini, M. Calandra, R. Car, C. Cavazzoni, D. Ceresoli, G. L. Chiarotti, M. Cococcioni, I. Dabo, A. Dal Corso, S. de Gironcoli, S. Fabris, G. Fratesi, R. Gebauer, U. Gerstmann, C. Gougoussis, A. Kokalj, M. Lazzeri, L. Martin-Samos, N. Marzari, F. Mauri, R. Mazzarello, S. Paolini, A. Pasquarello, L. Paulatto, C. Sbraccia, S. Scandolo, G. Sclauzero, A. P. Seitsonen, A. Smogunov, P. Umari and R. M. Wentzcovitch, *J. Phys.: Condens. Matter*, 2009, **21**, 395502.

36 M. Topsakal, H. Sahin and S. Ciraci, *Phys. Rev. B: Condens. Matter Mater. Phys.*, 2012, **85**, 155445.

37 O. Leenaerts, B. Partoens and F. M. Peeters, *Appl. Phys. Lett.*, 2008, **93**, 193107.

38 L. Tsetseris and S. T. Pantelides, *Carbon*, 2014, **67**, 58–63.

39 M. E. Suk and N. R. Aluru, *J. Phys. Chem. Lett*, 2010, **1**, 1590–1594.

40 S. Hu, M. Lozada-Hidalgo, F. C. Wang, A. Mishchenko, F. Schedin, R. R. Nair, E. W. Hill, D. W. Boukhvalov, M. I. Katsnelson, R. A. W. Dryfe, I. V. Grigorieva, H. A. Wu and A. K. Geim, *Nature*, 2014, **516**, 227–230.

41 K. K. Kim, A. Hsu, X. Jia, S. M. Kim, Y. Shi, M. Hofmann, D. Nezich, J. F. Rodriguez-Nieva, M. Dresselhaus, T. Palacios and J. Kong, *Nano Lett.*, 2012, **12**, 161–166.

42 Y. M. Shi, C. Hamsen, X. T. Jia, K. K. Kim, A. Reina, M. Hofmann, A. L. Hsu, K. Zhang, H. N. Li, Z. Y. Juang, M. S. Dresselhaus, L. J. Li and J. Kong, *Nano Lett.*, 2010, **10**, 4134–4139.

43 L. H. Li, E. J. G. Santos, T. Xing, E. Cappelluti, R. Roldan, Y. Chen, K. Watanabe and T. Taniguchi, *Nano Lett.*, 2015, **15**, 218–223.

44 R. V. Gorbachev, I. Riaz, R. R. Nair, R. Jalil, L. Britnell, B. D. Belle, E. W. Hill, K. S. Novoselov, K. Watanabe, T. Taniguchi, A. K. Geim and P. Blake, *Small*, 2011, **7**, 465–468.

45 H. A. Barham, S. A. Brahim, Y. Rozita and K. A. Mohamed, *Int. J. Electrochem. Sci.*, 2011, **6**, 181–198.

46 R. W. Revie, *Corrosion and Corrosion Control*, John Wiley & Sons, 2008, p. 25.

47 M. D. Wang, M. Y. Liu and J. J. Fu, *J. Mater. Chem. A*, 2015, **3**, 6423–6431.

48 J. Fu, T. Chen, M. Wang, N. Yang, S. Li, Y. Wang and X. Liu, *ACS Nano*, 2013, **7**, 11397–11408.

49 H. Gao, J. Zhang, M. Li, K. Liu, D. Guo and Y. Zhang, *Curr. Appl. Phys.*, 2013, **13**, 935–939.

50 M. H. Chou, S. B. Liu, C. Y. Huang, S. Y. Wu and C. L. Cheng, *Appl. Surf. Sci.*, 2008, **254**, 7539–7543.

51 Z. H. Gan, G. Q. Yu, B. K. Tay, C. M. Tan, Z. W. Zhao and Y. Q. Fu, *J. Phys. D: Appl. Phys.*, 2004, **37**, 81–85.

52 N. Cabrera and N. F. Mott, *Rep. Prog. Phys.*, 1949, **12**, 163–184.